Cortical Microcircuitry of Performance Monitoring

Amirsaman Sajad, **David C. Godlove**, and **Jeffrey D. Schall**

Department of Psychology, Vanderbilt Vision Research Center, Center for Integrative & Cognitive Neuroscience, Vanderbilt University, Nashville, TN

Abstract

Medial frontal cortex enables performance monitoring, indexed by the error-related negativity (ERN) and manifest by performance adaptations. In monkeys performing a saccade countermanding (stop signal) task, we recorded EEG over and neural spiking across all layers of the supplementary eye field (SEF), an agranular cortical area. Neurons signaling error production, feedback predicting reward gain or loss, and delivery of fluid reward had different spike widths and were concentrated differently across layers. Neurons signaling error or loss of reward were more common in layers 2 and 3 (L2/3), while neurons signaling gain of reward were more common in layers 5 and 6 (L5/6). Variation of error- and reinforcement-related spike rates in L2/3 but not L5/6 predicted response time adaptation. Variation in error-related spike rate in L2/3 but not L5/6 predicted ERN magnitude. These findings reveal novel features of cortical microcircuitry supporting performance monitoring and confirm one cortical source of the ERN.

Effective behavior requires evaluating the outcomes of actions and adapting performance to optimize consequences. The countermanding (stop signal) task affords investigation of performance monitoring and executive control[1], because humans and macaque monkeys performing saccade countermanding strategically adapt saccade latency according to performance outcomes[2].

Medial frontal cortex contributes to performance monitoring and executive control, but specific mechanisms remain uncertain[3,4]. Hypotheses have been tested using the noninvasive measure of the error-related negativity (ERN) in humans[5], which is also observed in macaque monkeys[6]. However, mechanistic hypotheses require information about neural spiking patterns across cortical layers[7]. It is well-known that neural spiking in anterior

---

cingulate cortex (ACC) contributes to performance monitoring by signaling errors and reinforcement gain and loss[8,9,10,11,12]. However, the supplementary eye field (SEF), an agranular area on the dorsomedial convexity in macaques, also contributes to performance monitoring and executive control by signaling errors and reinforcement[13,14,15]. SEF in macaques is homologous to SEF in humans, as SMA in macaques is homologous to SMA in humans[16]. Parallel evidence in humans has been found in the supplementary motor area[17]. SEF also signals proactive inhibition predicting whether movements will ultimately be inhibited[18], and subthreshold electrical stimulation of sites in SEF improves performance in the countermanding task by delaying the reaction time[19].

Information processing occurs through a canonical cortical microcircuit[20] but predictions from this circuit are based on sensory cortical areas having a granular layer 4. Previous work has shown that these predictions are contradicted in agranular areas like SEF[21,22,23,24]. Moreover, nothing is known about the laminar distribution of neural spiking in a medial frontal area of monkeys during demanding tasks. By showing how error, reward loss, and reward gain signals arise within and flow across SEF layers, we offer unprecedented details of the cortical microcircuitry supporting performance monitoring. By showing that the error signals and the balance of gain and loss signals in L2/3 but not L5/6 predict adaption of response time (RT), we constrain models of executive control. By showing how variation in error-related spiking in SEF predicts variation of ERN magnitude, we demonstrate that ACC is not the only source of the ERN.

Results

Countermanding performance and neural sampling

Neural data was recorded from two macaque monkeys performing the saccade countermanding task with explicit feedback tone cues (Fig. 1a)[25]. We acquired 33,816 trials (Monkey Eu: 11,583, Monkey X: 22,233) across 29 sessions. Both monkeys exhibited the typical sensitivity to the stop signal. The probability of failing to cancel the saccade on stop signal trials increased with stop signal delay. Response time (RT) was significantly shorter in noncanceled compared to no stop signal trials (Eu: $F(1,8467) = 424$, $p < 10^{-5}$; X: $F(1,17451) = 439$, $p < 10^{-5}$) and stop signal reaction time (SSRT) was of typical magnitude.

EEG was recorded with leads placed on the cranial surface by the chamber over medial frontal cortex, and a linear electrode array (Plexon, 150 μm spacing) was inserted in SEF perpendicular to the cortical layers (Fig. 1b). SEF was localized by anatomical landmarks and intracortical electrical microstimulation[22]. We recorded neural spiking in 29 sessions (Eu: 12, X: 17) sampling activity from five neighboring sites. Overall, 575 single units (Eu: 331, X: 244) were isolated of which 61 (Eu: 51, X: 10) were modulated after countermanding errors and 269 (Eu: 106, X: 163) were modulated after feedback about reinforcement gain or loss or when fluid reward was delivered. In 16 of the 29 sessions electrode arrays were oriented perpendicular to cortical layers. The description of the laminar distribution of various signals reported here is based on these sessions for which we could confidently assign neurons to different layers[2224] (Supplementary Fig. 1). Further support for the laminar assignments was provided by an analysis of the depths of SEF layers measured in histological sections visualized with Nissl, neuronal nuclear antigen (NeuN),

Gallyas myelin, acetylcholinesterase (AChE), nonphosphorylated neurofilament H (SMI-32), as well as the calcium-binding proteins parvalbumin (PV), calbindin (CB), and calretinin (CR)[27]. Additional information about laminar structure was assessed through the pattern of cross-frequency phase-amplitude coupling across SEF layers[24]. Due to variability in the estimates and the indistinct nature of the L6 border with white matter, some units appeared beyond the average gray-matter estimate; these were assigned to the nearest cellular layer. We sampled 293 neurons from these penetrations of which 173 (Eu: 65/104 neurons; X: 108/189) contributed to the results on laminar distribution of error-related and reinforcement-related monitoring signals (Supplementary Table 1).

Error signals

By design, monkeys produced noncanceled gaze shift errors on ~50% of stop signal trials, which comprised ~40% of all trials. Error-related neural spiking was identified as higher discharge rate on errant noncanceled trials compared to correct no stop signal trials starting within 250 ms following the saccade before the feedback tone (Fig. 2a; Supplementary Fig. 2). Only error trials in which the stop signal appeared before the saccade were considered. We now describe the functional architecture of Error neurons in SEF.

Functional properties of error signals—Error-related spiking was observed in multiple penetrations in both monkeys but was concentrated at particular locations (Chi-square contingency test of incidence across penetration locations, $\chi^2(4, N = 575) = 101.5$, p $< 10^{-5}$; Supplementary Table 1). This difference in prevalence of error-related neurons was found in both monkeys. Replicating previous findings, most error-related responses (45/61 neurons) were not lateralized, and the remainder exhibited similar modulation pattern for contra- and ipsiversive saccades. Roughly half of the Error neurons (32/61) showed similar patterns of modulation during other behaviors which resulted in a loss of opportunity to obtain reward (Supplementary Fig. 3). In our sample, error-related neurons were recruited beginning ~40 ms after error saccades, reached a maximum of ~90% recruitment at ~190 ms, and gradually reduced to ~30% of Error neurons active 500 ms after the saccade (Fig. 2b).

Using trough-to-peak duration of the action potential waveform, we inferred whether neurons were putative pyramidal neurons with broad spikes or interneurons with narrow spikes. Although allowing some misclassification[26], this information has been a useful heuristic. We found that the majority of Error neurons (52/61) were putative pyramidal neurons, while a minority were putative interneurons (Supplementary Fig. 4).

Laminar organization of error signal—The time-depth profile of error-related spiking was determined from 16 sessions with verified perpendicular penetrations for which we had confidence in the layer assignments (42/61 neurons). Fig. 2c shows the percentage of neurons at each depth exhibiting error-related modulation as a function of time, represented by the intensity of the color-map. The beginning of error activity varied across depth (Two-way ANOVA (session x depth) $F(2,41) = 4.99$, $p = 0.0132$). Post-hoc analysis shows that the latency of neurons in the middle layers (i.e., lower L3 and upper L5) are significantly shorter than those in upper layers ($t(31) = 3.56$, $p = 0.0036$, Bonferroni correction), and lower layers

(t(24) = 2.65, p = 0.042). There was no significant difference between L2/3 and L5/6 in onset of error activity (p = 0.61). Error neuron recruitment persisted in lower L3, L5, and lower L6 (Fig. 2c). Thus, Error neuron recruitment exhibited a distinct laminar pattern through time.

Neural spiking and the error-related negativity—We replicated the ERN as greater negative polarization on error relative to correct trials measured over medial frontal cortex[8]. It arose with similar latencies across monkeys (Eu: ~120-230 ms; X: ~120-190 ms (Fig. 3a; Supplementary Fig. 5). We examined the relationship between variation of the cranial EEG and variation of neural spiking in SEF. The relationship between neural events in SEF and the voltages measured on the cranium above SEF is both biophysical and statistical. The cranial voltage produced by synaptic currents associated with a given spike must follow Maxwell's equations as applied to the brain and head no matter what kind of trial a monkey is performing. Hence, we counted the spikes of Error neurons during the 50-200 ms post-saccadic period (referred to as A_{error}) separately in L2/3 and in L5/6. The conclusions do not change with spike counts in overlapping intervals of different durations. Error and correct trials are pooled together, controlling for categorical differences, but the reported pattern of relationships was observed when the trials were analyzed separately. A_{error} in L2/3 and in L5/6 were correlated (Spearman's correlation; $r_s(118) = 0.549$, $p < 10^{-5}$). To account for the variation of spike rate across error and correct trial types, we employed partial rank correlation. A_{error} in L2/3 was correlated with A_{error} in L5/6 (Partial rank correlation: $r_s(117) = 0.467$, $p < 10^{-5}$).

Given these correlations, we next evaluated the trial-by-trial relationship between variation of ERN magnitude and variation of A_{error} in L2/3 and in L5/6. Controlling for the variation of ERN polarization and spike rate across trial outcomes and the correlation of neural spiking across layers, we found that polarization magnitude variation of the ERN was negatively correlated with the variation of A_{error} in L2/3 but not in L5/6 (Fig. 3b; $r_s(116) = -0.568$, $p < 10^{-5}$, Supplementary Fig. 6). The relationship between ERN polarization and A_{error} in L2/3 but not in L5/6 was consistently observed on both correct and error trials separately (Supplementary Fig. 6, Supplementary Table 2). The variation of ERN polarization was not related to the activity of other types of SEF neurons (Supplementary Fig. 6).

Reinforcement signals

A feedback tone was presented 600±0 ms after no stop signal or noncanceled saccades, distinguishing correct from error performance. On correct trials juice reward was delivered 600 ± 0 ms after the tone. This temporal structure dissociated self-generated monitoring signals from responses to sensory cues. We now describe the functional architecture of reinforcement-related Gain and Loss neurons in SEF.

Functional signals related to feedback and reward—Reinforcement-related neural spiking was identified by comparing discharge rates between unrewarded and rewarded (no stop signal and canceled stop) trials in the period from feedback tone until 200 ms following scheduled delivery of the fluid reward. Any neuron with significant modulation in this

period was considered reinforcement-related (Fig. 4a, 4d; Supplementary Fig. 7). Neurons signaling feedback, reward anticipation or reward delivery were observed in both monkeys, at all recording sites (Supplementary Table 1). Most reinforcement-related neurons were modulated during one interval, but some were modulated in both the feedback and the reward intervals. Two major classes of reinforcement-related signals were observed, distinguished by their valence (Fig. 4b, 4e). Gain neurons exhibited higher discharge rates on rewarded than on unrewarded trials (110 modulation intervals in 91 neurons). This difference could result from either facilitation on rewarded trials (64/110), suppression on unrewarded trials (29/110), or both (17/110). Loss neurons exhibited higher discharge rate on unrewarded than on rewarded trials (247 modulation intervals in 189 neurons). This difference could result from either facilitation on unrewarded trials (86/247), suppression on rewarded trials (87/247), or both (74/247). Only 10% of reinforcement-related neurons also modulated after errors, evenly distributed between Gain and Loss neurons (Supplementary Fig. 7). The valence of modulation of Gain and Loss neurons were not conserved for non-task-related behaviors which resulted in a loss of opportunity to obtain reward (Supplementary Fig. 3).

Individual Gain and Loss neurons began modulating in the interval following the feedback tone until after expected reward delivery time. Both types were recruited monotonically until ~350 ms after the tone and sustained recruitment until 200 ms after reward delivery (Fig. 4b,e). Gain neurons were almost exclusively broad spike putative pyramidal neurons (85/91), but Loss neurons were comprised of both putative interneurons (43/189) and pyramidal neurons (146/189). Compared to Gain neurons, a higher proportion of Loss neurons were interneurons (Chi-square test, $\chi^2(1, N = 280) = 11.11$, p = 8.6×10^{-4}, Supplementary Fig. 7).

Laminar organization of gain and loss signals—In verified perpendicular penetrations we determined the laminar organization of gain and loss signals. Gain and Loss neurons were distributed significantly differently across cortical depth ($\chi^2(4, 158) = 12.86$, p = 0.012). In time-depth plots of the recruitment of Gain and Loss neurons we found that whereas Gain neurons were mainly observed in lower L3, L5 and L6 (Fig. 4c), Loss neurons had the highest density in L2/3 and lowest density in L5 and upper L6 (Fig. 4f). Thus, reinforcement processing in the SEF involved the counterbalanced activation of two pools of neurons with distinct laminar distributions. On rewarded correct trials, Gain neurons, densest in L5/6, were facilitated while Loss neurons, densest in L2/3, were suppressed (Fig. 5a). This difference in laminar distribution between facilitation and suppression in response to positive outcomes was significant ($\chi^2(1, 109) = 13.3$, p = 9.7×10^{-3}). On unrewarded error trials, Loss neurons in all layers were facilitated, while only a small proportion of Gain neurons, mainly in lower L3 and L5/6, were suppressed (Fig. 5b). The beginning of modulation of Gain and Loss neurons did not vary significantly across cortical depth.

Laminar modulation and executive control—We found that neural spiking in SEF was linked to adaptive control of countermanding performance. Both monkeys exhibited longer RT following errors (one sample t-test on sessions mean RT values, Eu: t(11) = 2.80, p = 0.017, X: t(16) = 4.70, p = 2.4×10^{-4}) and shorter RT following correct trials (Eu: t(11)

= −4.88, p = 4.9 × 10^{-4}, X: t(16) = −7.66, p < 10^{-5}) (Fig. 6). RT adaptation in the next trial (RT$_{n+1}$ - RT$_n$) differed significantly between the two conditions (paired t(28) = 9.25, p < 10^{-5}). To investigate the relationship between neural spiking on the current trial and RT adaptation, we counted the spikes produced after the saccade by Error neurons (A$_{error}$) and after reinforcement feedback by Gain (A$_{gain}$) and Loss (A$_{loss}$) neurons sampled in L2/3 and in L5/6 separately.

Controlling for correct and error trial outcome, we found a significant positive relationship between RT adaptation and the activity of Loss and Gain neurons (A$_{loss}$ - A$_{gain}$) across all layers in the feedback period (partial rank correlation, r$_s$(577) = 0.098, p = 0.018). Across trials, A$_{loss}$ - A$_{gain}$ in L2/3 was correlated with A$_{loss}$ - A$_{gain}$ in L5/6 (Spearman's correlation: r$_s$(258) = 0.45, p < 10^{-5}). Controlling for trial outcome and the correlation of neural spiking across layers, we found that RT adaptation was correlated significantly with A$_{loss}$ - A$_{gain}$ in L2/3 (r$_s$(256)= 0.13, p = 0.032) but not in L5/6 (Fig. 6b, Supplementary Fig. 8). Similarly, RT adaptation was correlated with A$_{error}$ in L2/3 but not in L5/6 (r$_s$(116) = 0.202, p = 0.028) (Fig. 6b, Supplementary Fig. 8). These results demonstrate layer-specific influences of SEF performance monitoring signals on RT adaptation.

Discussion

The results of this study offer unprecedented, new insights into the cortical microcircuitry supporting error and reward processing in medial frontal cortex of primates. Major patterns of neural spiking that signaled error, loss and gain replicated previous studies of SEF during saccade countermanding[13] and other tasks[15][27]. Beyond replication, these results provide the first information about the laminar distribution of different kinds of signals in a medial frontal area, which offers the first opportunity to determine how neural spiking across cortical layers can contribute to the ERN and to adaptive control of performance.

Error processing.

The countermanding task is very useful to explore performance monitoring including individual differences and addiction[28,29]. Noncanceled error trials occur, by design, in 50% of stop signal trials, which constitute ~40% of all trials. The noncanceled errors can be detected easily and are signaled by the presence of the ignored stop signal. In other tasks error can be rare, can entail the selection of the wrong choice alternative, and may not be accompanied by an external signal. Certainly, both approaches are complementary and neither disqualifies the other. Consequently, these data offer multiple new insights about error processing in SEF.

First, Error neurons were concentrated in some but not all penetrations, which implies that SEF can be organized in columnar modules. If so, further research is needed to determine what functions are segregated.

Second, most Error neurons had wide spikes, while some had narrow spikes. Some pyramidal neurons in macaque motor cortex can have narrow spikes due to expression of Kv3.1b potassium channel[26], but the expression of this channel in SEF is unknown. CR and CB neurons have relatively small somas concentrated in L2 and upper L3, while PV neurons

have larger somas distributed more uniformly from L2 to L6 in SEF[22]. Previously, we reported that the Plexon linear electrode array samples narrow spikes with approximately equal likelihood across SEF layers; therefore, we infer that the narrow spiking neurons described here are most commonly PV neurons. Overall, we found that narrow-spiking neurons were more commonly Error and Loss neurons signaling negative outcomes. The division of function between neurons with broad and narrow spikes that we describe in SEF is paralleled by differences in ACC[12].

Third, the distribution of error-related neural spiking in time and depth was not uniform across SEF layers. Error-related signals were observed earliest in deep L3 and upper L5, followed by sustained activation in L3, upper L5, and lower L6. This temporal pattern resembles the temporal pattern of current sinks observed in response to passive visual stimulation[27] and agrees with the general flow of signals suggested by the canonical cortical microcircuit[25].

We replicated previous observations of an ERN associated with error saccades in macaque monkeys performing saccade countermanding[6]. The timing of the ERN in the present study appears later than that often reported in studies requiring manual responses, but it matches that reported previously in humans performing the saccade countermanding task[30]. Particular conclusions follow from a functional relationship between SEF and the ERN. First, the association validates the interpretation of this neural spiking in terms of error monitoring and not some other operation or representation. Second, located on the dorsomedial convexity in macaque monkeys, SEF is ideally positioned to contribute to voltage polarizations recorded over medial frontal cortex. Further research is needed to determine how sharp are the boundaries between medial frontal areas monitoring actions of different effectors.

Origin of ERN.

These results provide new insights into the cortical sources of the ERN (Fig. 7a)[31]. We observed that variations in error-related (but no other neural spiking) in L2/3 but not in L5/6 predicted variation of EEG polarization across both error and correct trials. Because action potentials are not large or sustained enough to produce event-related potentials, we surmise that this neural spiking coincides with coherent current flow strong enough to produce in the ERN. How different patterns of current flow contribute to EEG voltage remains unresolved[32]. Perhaps, being closer to the EEG electrode, current in L2/3 of SEF has more impact than current in L5/6. Alternatively, synaptic activity producing the event-related potential on correct and error trials could originate from different sources. On correct trials a negative-going event-related potential is observed (see Fig. 3a), essentially concluding the readiness potential preceding movement. If the "correct related negativity" has a different source than the ERN[5], then synaptic input can be coherent among different neurons on different trials, so the correlation of spike rate variation and EEG voltage variation could hold for one but not the other kind of trial for a given neuron. Our finding of an association between SEF L2/3 spike rate and EEG on both error and correct trials argues against this possibility.

Other research indicates that ACC contributes to the ERN[7]. Thus, both SEF and ACC contribute to the ERN. This opens new research opportunities to understand biophysically how current dipoles with opposite polarities and different distances from the cranial surface sum to produce the ERN. This also has additional computational implications. If the ERN arises from multiple sources, then it likely manifests multiple computations and representations. If so, then no single, exclusive theory of the ERN is possible.

Reinforcement processing.

We found that secondary feedback and primary reward were signaled by both spike rate facilitation and suppression, as observed before[11][12]. Although Gain neurons resemble reward-related dopamine neurons[33] and Loss neurons, habenula neurons[34], the activity of both was more sustained than these subcortical exemplars, suggestive of additional cortical processing of this information. Gain neurons were more concentrated in L5/6, while Loss neurons were more concentrated in L2/3. Overall, many more neurons increased discharge rate following negative outcomes and decreased discharge rate following positive outcomes. The activity of Gain and Loss neurons can provide a neural substrate for reinforcement learning and performance monitoring. To verify this conjecture, future work should determine whether Gain and Loss neurons in different layers are influenced by factors such as confidence, prediction error, reward value, state, and surprise.

We found RT slowing after errors and RT speeding after correct trials. These adaptation effects are not found across every experiment and in all subjects performing the same task[2]. Nevertheless, in this study both monkeys exhibited common behavioral adaptations. Previous work demonstrated that subthreshold electrical stimulation of SEF improves saccade countermanding performance by delaying RT[19]. We found that, similar to error-related activity, the balance of activation of Gain and Loss neurons in L2/3 but not in L5/6 predicted RT adaptation in the next trial. The observed weak correlations between RT adaptation and spike rate modulation is further evidence that SEF influences but does not dictate responses. This laminar dissociation of processing is consistent with previous evidence for weak interlaminar processing in SEF[24]. We propose that the complementary modulation of Gain and Loss neurons can serve as a push-pull mechanism to adapt performance.

Extrinsic circuitry of monitoring and executive control.

This new information about the timing and laminar distribution of Error, Gain, and Loss neurons coupled with extensive knowledge about extrinsic inputs and outputs of SEF[35,36] suggest several specific hypotheses and associated research questions about how signals can arise in SEF and what influence they can have on performance (Fig. 7b).

SEF can receive reinforcement gain and loss signals via afferents from the dorsal segments of the substantia nigra and ventral tegmental area complex[37] or the locus coeruleus [38]. The laminar organization of these afferents in SEF is unknown, but the simultaneity of Gain and Loss signals across layers is consistent with diffuse termination spanning all layers.

SEF is innervated by the mediodorsal nucleus of the thalamus, terminating in deep L3[39] and can convey an efferent copy signal[40]. A recent model of agranular cortex[7] proposes that

errors can be detected through comparison of a task rule conveyed from dorsolateral prefrontal cortex and an efferent copy of the saccade command. Synaptic integration of these conflicting signals by L3 and L5 neurons can result in error-related spiking recorded from lower L3 and upper L5. Subsequent cortical processing produces later error-related spiking in L2 and L6. Neurons in L6 involved in sustained error and reinforcement processing project to the thalamus and can influence the processing of the efferent copy, perhaps resetting the circuit after the error is recognized. In the context of the saccade countermanding task, the anatomical and functional relationships revealed by these findings suggest that the abnormal countermanding performance[41] and abnormal ERN associated with schizophrenia[42] can arise from disruption of the efferent copy signal in schizophrenia[43].

Through L2/3 pyramidal neuron projections to other cortical areas, SEF will convey mainly error and loss signals. Previous research showed that error-related spiking in SEF preceded that in ACC[8]. Hence, further research is needed to characterize, for example, how much hierarchy and reciprocity occurs between medial frontal areas. A complete understanding of medial frontal performance monitoring will also need to account for differences in extrinsic and intrinsic neuron properties in SEF and ACC.

RT adaptation can be mediated by and through SEF, because SEF can influence saccade production through efferents to frontal eye field (FEF), caudate nucleus (CN), superior colliculus (SC), and brainstem oculomotor nuclei. Saccades are produced when activation from the SC and FEF to the brainstem saccade generator accumulates to a threshold, which triggers saccade initiation (Fig. 7b, inset). Based on previous findings[44], we suggest that speeding of saccade RT is accomplished by advancing the beginning of presaccadic activation, while slowing of RT is accomplished by delaying the beginning of presaccadic activation. Delaying RT increases the probability of success on stop signal trials by allowing more time for the STOP process to finish first, and vice versa. The magnitude of RT adaptation across trials was predicted by both the magnitude of the error signal and the balance of loss relative to gain signals only in L2/3, not in L5/6.

To enact such adaptations, we hypothesize that Gain neurons preferentially act through the direct pathway by innervating D1 neurons in the CN, which ultimately facilitate saccade production through the substantia nigra pars reticulata, while, Error and Loss neurons preferentially act through the indirect pathway by innervating D2 neurons, which ultimately inhibit saccade production through the GPe-STN pathway[45,46]. More research is needed to verify the laminar organization of medial frontal projections to CN and other targets in macaques. Error and Gain neurons in L5 that project to the SC, and Error, Gain, and Loss neurons in L6 that project to the thalamus can also support RT adaptations.

Intrinsic microcircuitry of monitoring and executive control.

Current models of executive control[34] and recent suggestions about agranular microcircuitry[7,23] motivate hypotheses about intrinsic processing in SEF (Fig. 7c). Given the density of CR, CB, and PV neurons in SEF, inhibition more prominently shapes processing in L2/3 than in L5/6. In agranular cortex, inhibition is predominantly intra-laminar, while

excitation is both inter- and intra-laminar but stronger from L2/3 to L5/6 than vice versa. This can explain the significantly weaker inter-laminar coupling in SEF compared to V1[24].

Error-related pyramidal neurons were found in L2/3 and L5/6, with samples of putative PV neurons in L3 and L5. Projections from L3 to L2 and from L2/3 and L5 to L6 can explain the laminar sequence of error-related activation observed. Recurrent connectivity can support the sustained error-related activation in L3, L5 and deep L6.

Reinforcement outcome was signaled by counterbalanced representations of reward gain and loss. Gain-related pyramidal neurons were found in deep L3 and L5/6. Loss-related pyramidal neurons were found in L2, 3, and 6. The pronounced suppression of a subpopulation of Gain and Loss neurons indicates that they receive GABAergic inputs from inhibitory interneurons. The majority of narrow-spiking putative PV neurons were Loss neurons, found in all layers. Hence, inhibition from these neurons can produce the suppression of Gain neurons in L3, 5, and 6. However, given that suppression of Loss neurons was concentrated in the L2/3 and that we encountered no narrow-spiking Gain neurons, we hypothesize that suppression of Loss neurons is mediated by CB and CR inhibitory neurons that were not sampled given their small somas.

To summarize, errors, negative feedback, and absence of reward elicit activity among pyramidal Loss neurons, spreading throughout L2/3 and L5/6. These neurons in turn activate PV cells in both L2/3 and L5/6, which inhibit intra-laminar Gain neurons. On the other hand, success, positive feedback, and delivery of reward elicit activity among pyramidal Gain neurons and suppression of Loss neurons.

Conclusion.

By highlighting many avenues for further research, these results demonstrate the tractability of formulating models of the microcircuitry of performance monitoring. Such models require filling many specific gaps in our knowledge. Fortunately, methods are available to obtain the required information. Such models can be firmly grounded on interactive race models of countermanding performance[47]. Deep insights into the microcircuitry and mechanisms of primary visual cortex began by describing the properties of neurons in different layers[48]. The current study provides the first equivalent information for the SEF. Being an agranular area, comparisons and contrasts with primary sensory areas provide insights into the degree of uniformity of cortical areas. As a likely source contributing to the ERN, details about laminar processing in SEF offer unprecedented insights into the microcircuitry of performance monitoring.

Methods

Monkey care, cortical mapping, and electrode placement

All procedures were approved by the Vanderbilt Institutional Animal Care and Use Committee in accordance with the United States Department of Agriculture and Public Health Service Policies on Humane Care and Use of Laboratory Animals. Methods were described previously[27]; here we summarize essential information before elaborating new

analyses. Data were collected from two macaque monkeys (Eu, M. radiata, male, 8.8 kg, ~6 years old; X, M. mulatta, female, 6 kg, ~8 years old).

To guide placement of recording chambers, structural MR images were acquired with a Philips Intera Achieva 3 tesla scanner using SENSE Flex-S surface coils placed above and below the head. T1-weighted gradient-echo structural images were obtained with a 3D turbo field echo anatomical sequence (TR = 8.729 ms; 130 slices, 0.70 mm thickness). Cilux recording chambers (Crist Instruments, Hagerstown, MD) were implanted normal to the cortex (17° for Eu, 9° for X relative to stereotaxic vertical) centered on midline 30 mm (Eu) and 28 mm (X) anterior to the interaural line.

The SEF is located in the dorsal medial convexity in macaques, making it readily accessible for laminar electrode array recordings perpendicular to the cortical layers. The single unit data reported here are from 29 penetrations sampling activity from five recording sites, two in Monkey Eu and three in monkey X. Three out of five were perpendicularly penetrated into the cortex (Supplementary Fig. 1). In monkey Eu, the perpendicular penetrations sampled data at site P1 located 31 mm anterior to the interaural line and 5 mm lateral to the midline. In monkey X the perpendicular recordings were obtained from site P2 and P3 located 5 mm lateral and 29 and 30 mm anterior, respectively. Chambers implanted over medial frontal cortex were mapped using tungsten microelectrodes (2-4 MΩ, FHC, Bowdoin, ME) to apply 200 ms trains of biphasic microstimulation (333 Hz, 200 μs pulse width). SEF was identified as the area from which saccades could be elicited using <50 μA of current. The positions affording access to SEF perpendicular to the cortical layers were located with MR and verified through mapping the three-dimensional orientation of neural activity as a function of depth. To confirm that these coordinates placed electrodes perpendicular to gray matter, we conducted CT scans with guide tubes in place and co-registered these data with structural MR images using a point-based method implemented in OsiriX (Geneva Switzerland). Images were reconstructed at $512 \times 512 \times 512$ with a voxel size of $0.252 \times 0.252 \times 0.122$ mm^3. The pial and white matter boundaries of the cortex were segmented in coronal and sagittal slices directly beneath the guide tube for each monkey transferred to the co-registered CT data. A custom algorithm determined angles perpendicular to the gray matter boundaries.

Electrophysiological data collection

During recordings, monkeys sat in enclosed primate chairs with heads restrained 45 cm from a CRT monitor (Dell P1130, background luminance of 0.10 cd/m^2, 70 Hz) subtending 46° x 36° of visual angle. Daily recording protocols were consistent across monkeys and sessions. After advancing the electrode array to the desired depth, 3-4 hours elapsed to allow stabilized recordings. This waiting period resulted in consistently stable recordings; single units could usually be held indefinitely. For this report, the monkeys performed ~2000-3000 trials of a saccade stop signal task.

EEG was recorded from the cranial surface with electrodes located over medial frontal cortex[8]. Electrodes were referenced to linked ears using ear-clip electrodes (Electro-Cap International). The EEG from each electrode was amplified with a high-input impedance head stage (Plexon) and bandpass filtered between 0.7 and 170 Hz.

Intracranial data were recorded using a 24-channel U-probe (Plexon, Dallas, TX) with 150 μm inter-electrode spacing. The U-probes had 100 mm probe length with 30 mm reinforced tubing, 210 μm probe diameter, 30° tip angle, 500 μm to first contact. Contacts were referenced to the probe shaft, and grounded to the metal headpost. All data were streamed to a data acquisition system (MAP, Plexon, Dallas, TX). Time stamps of trial events were recorded at 500 Hz. Eye position data were streamed to the Plexon computer at 1 kHz using an EyeLink 1000 infrared eye-tracking system (SR Research, Kanata, Ontario, Canada). LFP and spiking data were processed with unity-gain high-input impedance head stages (HST/32o25-36P-TR, Plexon). LFP data were bandpass filtered at 0.2-300 Hz and amplified 1000 times with a Plexon preamplifier, and digitized at 1 kHz. Spiking data were bandpass filtered between 100 Hz and 8 kHz and amplified 1000 times with a Plexon preamplifier, filtered in software with a 250 Hz high-pass filter and amplified an additional 32,000 times. Waveforms were digitized from −200 to 1200 μs relative to threshold crossings at 40 kHz. Thresholds were typically set at 3.5 standard deviations from the mean. Single units were sorted online using a software window discriminator and refined offline using principal components analysis implemented in Plexon offline sorter.

Statistics

No statistical methods were used to predetermine sample size, but our sample sizes are similar to those reported in previous publications[22][49,50]. Data distribution was assumed but not formally tested to be normal unless otherwise stated, when non-parametric tests were performed. Task conditions were pseudo-randomly presented. We did not select the type of neurons during data acquisition; all well-isolated neurons were analyzed. Data collection and analysis were not performed blind to the experimental conditions. No animals were excluded from the study. Data from all recording sites were included. For analyses on layer-specific activity, only sessions with perpendicular penetrations in the cortex were used. All statistical procedures for behavioral and neural data analysis were done using two-tailed tests unless otherwise specified. All statistics were performed using commercial softwares Matlab 2016/2017 (MatWorks Inc; Natick, MA, USA) and R: A language and environment for statistical computing (R Foundation for Statistical Computing; Vienna, Austria, http://www.R-project.org/).

Depth alignment and laminar assignment

We used depth alignments across sessions described previously[27]. Recording depths varied across session. Microdrive depth measures are not sufficiently reliable because they do not account for variable cortical dimpling. Hence, we aligned and averaged consecutive recording sessions relative to the peak of the initial visually evoked sink in current that is readily apparent in the current source density (CSD) pattern following presentation of a flashed visual stimulus. To account for low signal-to-noise ratio compared to that in primary visual cortex we devised an automated depth alignment procedure to minimize differences between recording sessions using all available current source and sink information in a given time window. Using the minimum of the initial visually-evoked sink in L3 as the zero-depth measure, this method identified the following depths as laminar boundaries: L1 to L2/3 at 0.21 mm, L3 to L5 at 0.36 mm, and L5 to L6 at 1.02 mm. Blurring of these boundaries will occur when the alignment of individual recording sessions deviates from that of the grand-

averaged CSD. Inspection of the alignment of individual sessions indicates that this blurring was minimal (Supplementary Fig. 1).

Analysis of neural spiking

All measurements of neural spiking were based on spike density functions (SDF) produced by convolving the spike train with a kernel resembling a postsynaptic potential defined by $SDF(t) = [1 - e^{(-t/\tau_g)}] * e^{(-t/\tau_d)}$ with growth time constant (τ_g) of 1 ms, and decay time constant (τ_d) of 20ms, corresponding to the values measured for excitatory post-synaptic potentials. Trials included in the calculation had at least one spike during the interval from 600 ms before target presentation until 900 ms after the feedback tone.

Error-related activity—Error-related activity was identified by comparing the SDF between error noncanceled trials and correct no stop signal trials. Error trials in which the stop signal appeared after the saccade were not included in this analysis. Periods of significant difference were defined when the difference between SDF on error and correct trials (referred to as difference function) exceeded 2 S.D. above a baseline difference measured during the 300 ms period before target presentation and persisted for at least 100 ms, or for 50 ms if the difference exceeded 6 S.D. above the baseline. Only saccades from the two trial types with similar RT (within 10 ms) and direction were used for comparison.

On some sessions after the error saccade, monkeys occasionally shifted gaze back to the fixation point. These trials were excluded unless this resulted in too few trials for meaningful interpretation of neural spiking. In this case, additional tests were performed to exclude the possibility that these movements influenced the results (Supplementary Fig. 2). First, we tested whether the beginning of differential activity shifted with the timing of the second saccade or remained synchronized on the error saccade. Error trials were divided into those with the shortest and the longest intersaccade intervals. Then, the slope between the onset of differential activity and median intersaccade interval in each group was calculated. If the slope of the line was <0.5, the putative error activity was classified instead as saccade-related. Second, we confirmed that removal of trials with the second saccade maintained the polarity of the difference function.

Reinforcement-related activity—Reinforcement-related unit activity was identified by comparing the SDF between rewarded no stop signal and unrewarded noncanceled saccade trials in the interval between the onset of the reinforcement tone and 200 ms after the instant of juice delivery on rewarded trials. Periods of significant difference were defined when the difference between SDF on error and correct trials (i.e., difference function) exceeded 2 S.D. Differential activity was only considered reinforcement-related if the difference between rewarded canceled and unrewarded noncanceled trials in this period had the same polarity and was statistically significant (spike count comparison, unpaired Wilcoxon test, $p < 0.05$).

To control for activity related to saccades during the feedback period, we took advantage of the lack of correspondence between the number of saccades in the post-tone period and trial outcome. This allowed us to reject putative reinforcement-related modulations if their strength did not correlate with the proportion of rewarded trials. First, we determined the time interval of significant differential activity. Then, through bootstrapping ($n = 1000$) we

randomly selected a subset of trials from the total set of rewarded no stop signal trials and unrewarded noncanceled trials. We measured the area under the SDF and the total number of saccades in this interval and calculated the percentage of rewarded trials. If the partial correlation between neural spiking and proportion of rewarded trials given the number of saccades was significant, then the modulation was considered significant for reward.

RT matching—Monkeys exhibited different RT across saccade directions. Therefore, for any analysis that involved a comparison in neural activity between two conditions, RTs were matched across same-direction saccades with 10 ms resolution. If multiple matching saccade RTs occurred, the trial with the closest timestamp in the session was selected.

Time-depth plots—To illustrate the temporal recruitment of neurons through cortical depth, we divided the number of recruited neurons at each point in time by the total number of neurons recorded at that depth (Supplementary Fig. 1c). Recruitment was defined as the time when the difference function was significant.

Quantification of the ERN

The ERN was determined from unfiltered EEG signals. High frequency noise was eliminated through averaging. The ERN was calculated from the grand average EEG following correct and error saccades. Only saccades with matching RT across the two conditions were included. The same trials were included for measurements of ERN and error-related modulation.

Single trial ERN magnitude was the voltage at the time of maximum polarization of the grand average ERN (monkey Eu: 187ms; monkey X: 147ms) subtracted from the voltage −50 ms before saccade initiation. We obtained results supporting the same conclusions if we did not subtract the pre-saccadic voltage.

Partial Correlation Analysis

Relationship between ERN and neural spiking—Single trial ERN amplitudes were normally distributed, with partially overlapping values on error and correct trials (Supplementary Fig. 4). Single trial neural spiking values, using only data from confirmed perpendicular penetrations, was the number of spikes recorded from neurons in L2/3 and in L5/6 50-200 ms following saccades, which included the majority of error-related spikes.

Outliers more than 3 standard deviations from the mean were removed from the EEG and spike data (Supplementary Fig. 4c). To account for inter-session variations in ERN voltage and spike counts, a fixed-effects adjustment was performed by centering each distribution on its median and dividing by its most extreme value. To ensure effective normalization using the fixed-effect adjustment, only sessions with >10 summed spike counts in L2/3 and L5/6 were used.

To examine the relationship between the EEG magnitude and the spiking activity, we conducted partial rank correlations on normalized data pooled across all sessions with a perpendicular penetration. Three factors were considered: (1) Spiking activity in L2/3, (2) spiking activity in L5/6, and (3) trial outcome. Trial outcome must be included to ensure that

any relationship between the ERN and neural spiking is not just because Error neuron activity and the EEG are different on error than correct trials by definition. Inclusion of interaction terms in the partial correlation did not alter the main results.

To measure the ERN magnitude more robustly, we grouped rank-ordered single-trial ERN values into 20 successive bins, which consisted of 15.1 ± 5.3 (mean $\pm$ SD) trials (Supplementary Fig. 4d). From trials in each bin we calculated the mean ERN magnitude (dependent variable), the mean spike count (independent variable), and the fraction of error trials (dummy variable values for trials in each bin). Data from all sessions was combined for a pooled partial correlation. Non-parametric Spearman correlations were used because linearity in relationships could not be assumed. Each point in Figure 3 plots the paired values of the rank of the normalized EEG voltage and the rank of the normalized spike count for each bin for every session.

Relationship between RT adaptation and neural spiking—RT adaptation was calculated as the difference in RT between the next and the current trial ($RT_{n+1} - RT_n$). To account for incidental lateralized asymmetries of RT, RT adaptation was measured only for trial pairs with same-direction saccades. To investigate the relationship between RT adaptation and neural spiking, the binning and partial rank correlation procedures described above were performed. Spike counts to obtain $A_{loss} - A_{gain}$ were based on the interval when Gain and Loss neurons showed significant modulation. First, the number of action potentials of Loss and Gain neurons were subtracted from each other, and the resultant values were normalized using the fixed effect adjustment described above. For the laminar relationship of RT adaptation with $A_{loss} - A_{gain}$ only sessions with Gain and Loss neurons in both L2/3 and L5/6 were used (13/16 sessions).

Each point in Figure 6 plots the paired values of the rank of the normalized RT adaptation and the rank of the normalized spike count for each bin for every session.

Supplementary Material

Refer to Web version on PubMed Central for supplementary material.

Acknowledgments

References

1. Verbruggen F, Logan GD. Models of response inhibition in the stop-signal and stop-change paradigms. Neurosci Biobehav Rev. 33:647–661 (2009). [PubMed: 18822313]

2. Emeric EE, Brown JW, Boucher L, Carpenter RH, Hanes DP, Harris R, Logan GD, Mashru RN, Paré M, Pouget P, Stuphorn V, Taylor TL, ,Schall JD. Influence of history on saccade

countermanding performance in humans and macaque monkeys. Vision Res. 47:35–49 (2007). [PubMed: 17081584]

3. Kolling N, Wittmann MK, Behrens TE, Boorman ED, Mars RB, Rushworth MF. Value, search, persistence and model updating in anterior cingulate cortex. Nat Neurosci. 19:1280–1285 (2016). [PubMed: 27669988]

4. Shenhav A, Cohen JD, Botvinick MM. Dorsal anterior cingulate cortex and the value of control. Nat Neurosci. 19:1286–1291 (2016). [PubMed: 27669989]

5. Gehring WJ, Liu Y, Orr JM, & Carp J The error-related negativity (ERN/Ne) In Luck SJ, & Kappenman E (eds.), Oxford handbook of event-related potential components (pp. 231–291). New York: Oxford University Press (2012).

6. Godlove DC, Emeric EE, Segovis CM, Young MS, Schall JD, Woodman GF (2011) Event-related potentials elicited by errors during the stop-signal task. I. Macaque monkeys. J Neurosci. 31:15640–15649. [PubMed: 22049407]

7. Cohen MX. (2014) A neural microcircuit for cognitive conflict detection and signaling. Trends Neurosci. 37:480–490. [PubMed: 25034536]

8. Ito S, Stuphorn V, Brown JW, Schall JD (2003) Performance monitoring by the anterior cingulate cortex during saccade countermanding. Science 302:120–2. [PubMed: 14526085]

9. Emeric EE, Brown JW, Leslie M, Pouget P, Stuphorn V, Schall JD (2008) Error related local field potentials in the medial frontal cortex of primates: Anterior cingulate cortex. Journal of Neurophysiology 99:759–772. [PubMed: 18077665]

10. Cai X, Padoa-Schioppa C. (2012) Neuronal encoding of subjective value in dorsal and ventral anterior cingulate cortex. J Neurosci. 32:3791–808. [PubMed: 22423100]

11. Monosov IE. (2017). Anterior cingulate is a source of valence-specific information about value and uncertainty. Nature Communications, 8:134.

12. Kawai T, Yamada H, Sato N, Takada M, & Matsumoto M (2018) Preferential representation of past outcome information and future choice behavior by putative inhibitory interneurons rather than putative pyramidal neurons in the primate dorsal anterior cingulate cortex. Cerebral Cortex. doi: 10.1093/cercor/bhy103. [Epub ahead of print]

13. Stuphorn V, Taylor TL, Schall JD (2000) Performance monitoring by the supplementary eye field. Nature 408:857–860. [PubMed: 11130724]

14. Emeric EE, Leslie M, Pouget P, Schall JD. (2010) Performance monitoring local field potentials in the medial frontal cortex of primates: Supplementary eye field. J Neurophysiol. 104:1523–1537. [PubMed: 20660423]

15. Chen X, Stuphorn V. (2015) Sequential selection of economic good and action in medial frontal cortex of macaques during value-based decisions. Elife. 4 pii: e09418. [PubMed: 26613409]

16. Amiez C, Petrides M. (2009) Anatomical organization of the eye fields in the human and non-human primate frontal cortex. Prog Neurobiol. 89:220–230. [PubMed: 19665515]

17. Bonini F, Burle B, Liégeois-Chauvel C, Régis J, Chauvel P, Vidal F. (2014) Action monitoring and medial frontal cortex: Leading role of supplementary motor area. Science. 343:888–891. [PubMed: 24558161]

18. Stuphorn V, Brown JW, Schall JD (2010) Role of supplementary eye field in saccade initiation: Executive, not direct, control. J Neurophysiol 103:801–816. [PubMed: 19939963]

19. Stuphorn V, Schall JD (2006) Executive control of countermanding saccades by the supplementary eye field. Nat Neurosci. 9:925–931. [PubMed: 16732274]

20. Bastos AM, Usrey WM, Adams RA, Mangun GR, Fries P, Friston KJ. (2012) Canonical microcircuits for predictive coding. Neuron. 76:695–711. [PubMed: 23177956]

21. Shipp S (2005) The importance of being agranular: a comparative account of visual and motor cortex. Philosophical Transactions of the Royal Society B: Biological Sciences 360:797–814.

22. Godlove DC, Maier A, Woodman GF, Schall JD. (2014) Microcircuitry of agranular frontal cortex: testing the generality of the canonical cortical microcircuit. J Neurosci. 2014 34:5355–69. [PubMed: 24719113]

23. Beul SF, Hilgetag CC (2014) Towards a "canonical" agranular cortical microcircuit. Frontiers in neuroanatomy, 8.

24. Ninomiya T, Dougherty K, Godlove DC, Schall JD, Maier A. (2015) Microcircuitry of agranular frontal cortex: contrasting laminar connectivity between occipital and frontal areas. J Neurophysiol. 113:3242–55 [PubMed: 25744881]

25. Hanes DP, Schall JD (1995) Countermanding saccades in macaque. Vis Neurosci 12:929–937. [PubMed: 8924416]

26. Vigneswaran G, Kraskov A, & Lemon RN (2011). Large identified pyramidal cells in macaque motor and premotor cortex exhibit "thin spikes": Implications for cell type classification. Journal of Neuroscience, 31:14235–14242. [PubMed: 21976508]

27. Kawaguchi N, Sakamoto K, Saito N, Furusawa Y, Tanji J, Aoki M, Mushiake H. (2015) Surprise signals in the supplementary eye field: rectified prediction errors drive exploration-exploitation transitions. J Neurophysiol. 113:1001–14. [PubMed: 25411455]

28. Stahl J, Gibbons H. (2007) Dynamics of response-conflict monitoring and individual differences in response control and behavioral control: an electrophysiological investigation using a stop-signal task. Clin Neurophysiol. 118:581–596. [PubMed: 17188565]

29. Chang A, Chen CC, Li HH, Li CS. (2014) Event-related potentials for post-error and post-conflict slowing. PLoS One. 9:e99909. [PubMed: 24932780]

30. Reinhart RM, Carlisle NB, Kang MS, Woodman GF (2012). Event-related potentials elicited by errors during the stop-signal task. II: Human effector-specific error responses. Journal of Neurophysiology, 107: 2794–2807. [PubMed: 22357790]

31. Cohen MX. (2017). Where does EEG come from and what does it mean? Trends in Neurosciences, 40:208–218. [PubMed: 28314445]

32. Riera JJ, Ogawa T, Goto T, Sumiyoshi A, Nonaka H, Evans A, Miyakawa H, Kawashima R. (2012) Pitfalls in the dipolar model for the neocortical EEG sources. Journal of Neurophysiology, 108:956–975 [PubMed: 22539822]

33. Schultz W (2000). Multiple reward signals in the brain. Nature Reviews Neuroscience, 1:199. [PubMed: 11257908]

34. Matsumoto M, Hikosaka O. Representation of negative motivational value in the primate lateral habenula. Nature Neurosci. 2009; 12:77–84. [PubMed: 19043410]

35. Huerta MF, Kaas JH (1990) Supplementary eye field as defined by intracortical microstimulation: connections in macaques. J Comp Neurol 293:299–330. [PubMed: 19189718]

36. Parthasarathy HB, Schall JD, Graybiel AM. (1992) Distributed but convergent ordering of corticostriatal projections: analysis of the frontal eye field and the supplementary eye field in the macaque monkey. J Neurosci. 12:4468–88. [PubMed: 1279139]

37. Williams SM, Goldman-Rakic PS. (1998) Widespread origin of the primate mesofrontal dopamine system. Cereb Cortex. 8:321–345. [PubMed: 9651129]

38. Aston-Jones G, Cohen JD. (2005) Adaptive gain and the role of the locus coeruleus-norepinephrine system in optimal performance. J Comp Neurol. 493:99–110. [PubMed: 16254995]

39. Giguere M, Goldman-Rakic PS. (1988) Mediodorsal nucleus: areal, laminar, and tangential distribution of afferents and efferents in the frontal lobe of rhesus monkeys. J Comp Neurol. 277:195–213. [PubMed: 2466057]

40. Sommer MA, Wurtz RH. (2008) Brain circuits for the internal monitoring of movements. Annu Rev Neurosci. 31:317–38. [PubMed: 18558858]

41. Thakkar KN, Schall JD, Boucher L, Logan GD, Park S (2011) Response inhibition and response monitoring in a saccadic countermanding task in schizophrenia. Biological Psychiatry 69:55–62. [PubMed: 20970778]

42. Foti D, Kotov R, Bromet E, Hajcak G. (2012) Beyond the broken error-related negativity: functional and diagnostic correlates of error processing in psychosis. Biol Psychiatry. 71:864–872. [PubMed: 22336564]

43. Thakkar KN, Diwadkar VA, Rolfs M. (2017) Oculomotor prediction: A window into the psychotic mind. Trends Cogn Sci. 21:344–356. [PubMed: 28292639]

44. Pouget P, Logan GD, Palmeri TJ, Boucher L, Paré M, Schall JD. (2011) Neural basis of adaptive response time adjustment during saccade countermanding. J Neurosci. 31:12604–12612. [PubMed: 21880921]

45. Kravitz AV, Tye LD, Kreitzer AC. (2012) Distinct roles for direct and indirect pathway striatal neurons in reinforcement. Nat Neurosci. 15:816–818. [PubMed: 22544310]

46. Vicente AM, Galvão-Ferreira P, Tecuapetla F, Costa RM. (2016) Direct and indirect dorsolateral striatum pathways reinforce different action strategies. Curr Biol. 26:R267–269. [PubMed: 27046807]

47. Boucher L, Palmeri TJ, Logan GD, Schall JD (2007) Inhibitory control in mind and brain: an interactive race model of countermanding saccades. Psychol Rev 114:376–97. [PubMed: 17500631]

48. Hubel DH, Wiesel TN. (1968) Receptive fields and functional architecture of monkey striate cortex. J Physiol. 195:215–243. [PubMed: 4966457]

49. Chandrasekaran C, Peixoto D, Newsome WT, & Shenoy KV Laminar differences in decision-related neural activity in dorsal premotor cortex. Nature Communications, 8, 614 (2017).

50. Bastos AM, Loonis R, Kornblith S, Lundqvist M, Miller EK. Laminar recordings in frontal cortex suggest distinct layers for maintenance and control of working memory. Proc Natl Acad Sci U S A. 115, 1117–1122 (2018). [PubMed: 29339471]
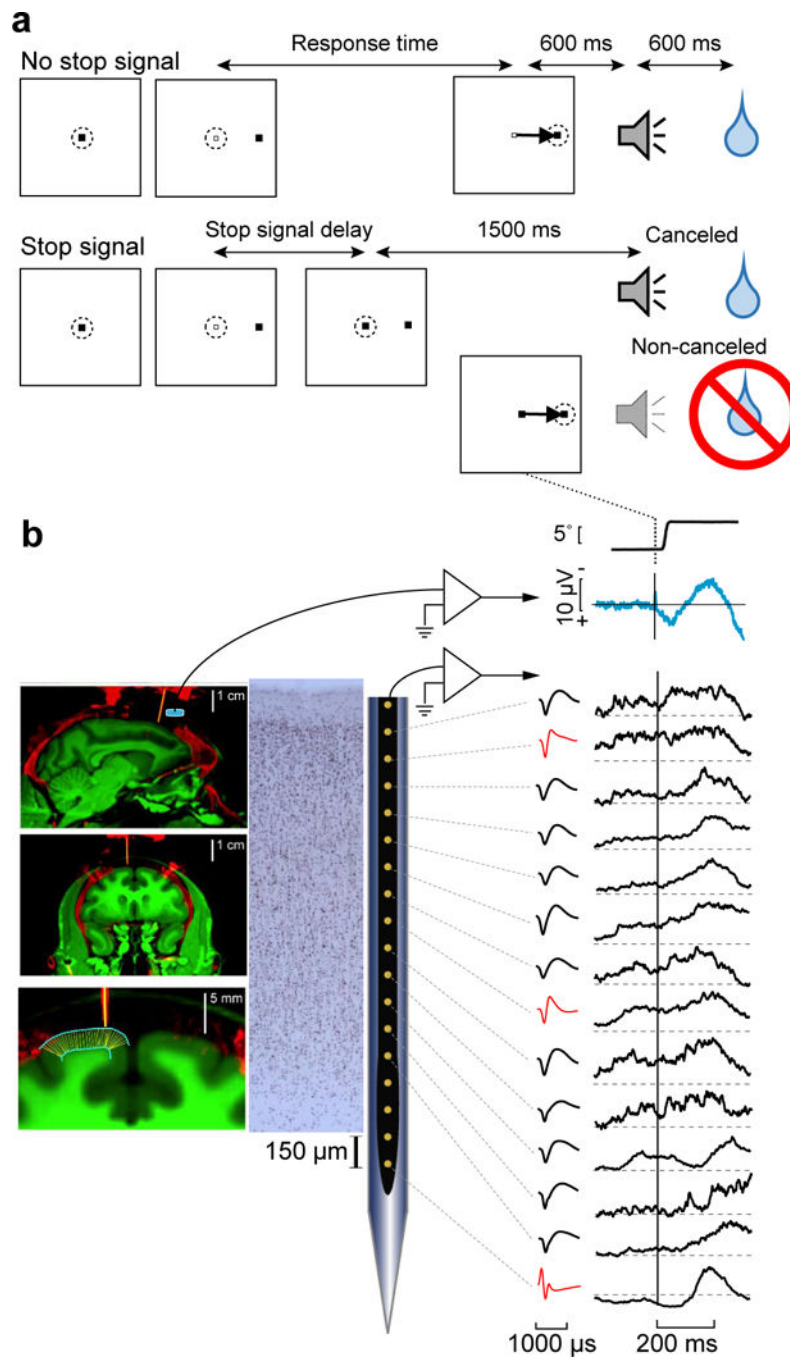
Fig. 1 |. Experimental procedures.

a, Saccade countermanding task. Monkeys initiated trials by fixating a central point. After a variable time, the center of the fixation point was extinguished. A peripheral target was presented simultaneously at one of two possible locations. On no stop signal trials monkeys were required to shift gaze to the target, whereupon after 600 ± 0 ms a high-pitch auditory feedback tone was delivered, and 600 ± 0 ms later fluid reward was provided. On stop signal trials (~40% of trials) after the target appeared, the center of the fixation point was re-illuminated after a variable stop signal delay, which instructed the monkey to cancel the

saccade in which case the same high-pitch tone was presented after a $1,500 \pm 0$ ms hold time followed after 600 ± 0 ms by fluid reward. Stop signal delay was adjusted such that monkeys successfully canceled the saccade in ~50% of trials. In the remaining trials, monkeys made noncanceled errors, which were followed after 600 ± 0 ms by a low-pitch tone, and no reward was delivered. Monkeys could not initiate trials earlier after errors. **b,** EEG was recorded from the cranial surface using an electrode (blue cylinder) positioned over the medial frontal cortex while neural spiking was sampled from all cortical layers with a linear electrode array oriented perpendicular to the cortical layers (thick yellow). Coregistered MR (green), showing gray and white matter, and CT (red), showing bone, implanted stainless steel chamber and other hardware including guide tubes in sagittal (top), and coronal (middle, bottom) planes. Bottom panel illustrates outcome of algorithm to segment gray matter (cyan) and determine radial lines (thin yellow). Spiking activity was recorded across all cortical layers (left) using Plexon U-probe. Neuron density is shown in Neun stained section. Neurons with both broad (black) and narrow (red) spikes were sampled (middle). Aligned on noncanceled saccades are plotted the average EEG, with associated spike potential artifact, and simultaneous spike density functions in all layers exhibiting various patterns of elevated discharge rates after the error.
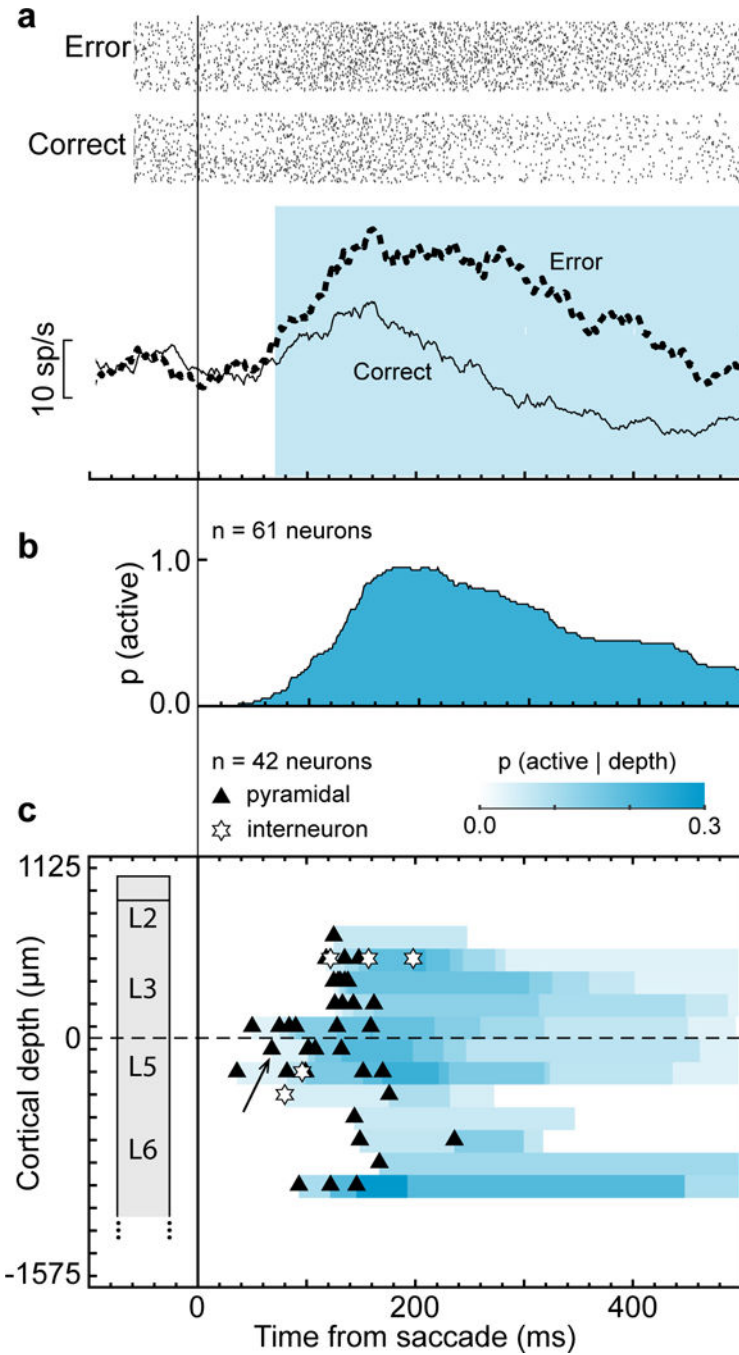
Fig. 2 |. Time-depth organization of error-related spiking in SEF.
a, Representative neuron with greater discharge rate following error noncanceled (dotted) relative to correct (solid) saccades. This neuron was located in superficial layer 5 and had a broad spike. Rasters show activity for error noncanceled and latency-matched correct no stop signal trials. Cyan highlights duration of significant error-related modulation. **b,** Recruitment of Error neuron signal through time after saccade across all sessions. **c,** Time-depth plot showing latency and proportion of recruited Error neurons through time at each depth from perpendicular penetrations. Symbols mark beginning of error-related modulation

for neurons with spike width 250 μm (black triangles) and < 250 μm (white stars). The representative neuron in **a** is indicated by the black arrow. Color map indicates the percentage of neurons signaling an error through time at each depth. Dashed horizontal line marks L3-L5 boundary. The lower boundary of L6 is not discrete.
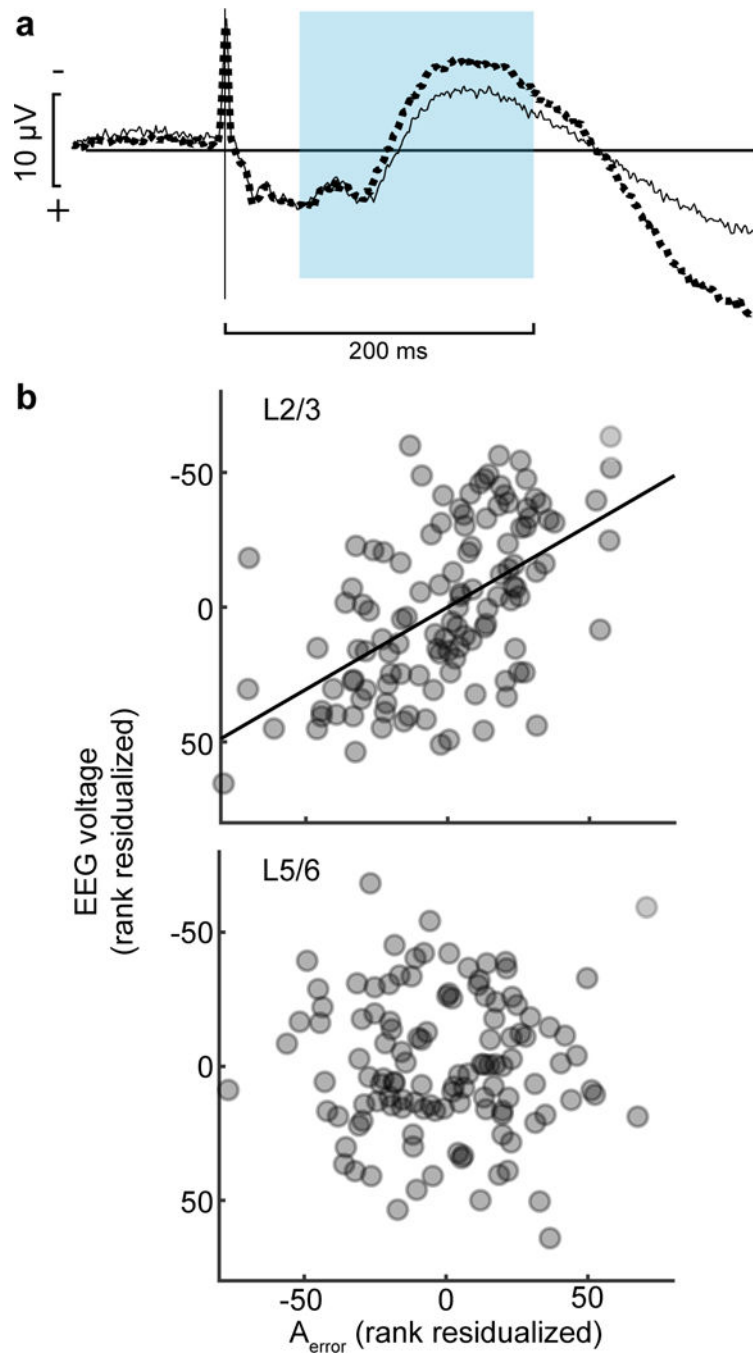
Fig. 3 |. Relationship between error-related neural spiking and error-related negativity.
a, Grand average EEG on correct (solid) and error (dotted) trials obtained from all 29
sessions. Saccade spike potential is prominent in both, but polarization is initially
significantly more negative following errors, characteristic of the ERN, followed by greater
positivity. Shaded area highlights the period in which spikes were counted. **b,** From 6
sessions with perpendicular penetrations, relationship between EEG voltage and spike count
for Error neurons (Aerror) recorded in L2/3 (top) and L5/6 (bottom). Along the ordinate
scale is plotted, according to EEG convention, the residual fixed-effects-adjusted EEG

voltage ranks controlling for the ranks of fixed-effects-adjusted activity in the opposite layer and the probability of an error. Along the abscissa scale is plotted the residual fixed-effects adjusted A_{error} rank in the identified layer controlling for the fixed-effects adjusted activity in the opposite layer and the probability of an error. Each point plots the average EEG voltage and associated spike count in one of 20 bins with equal numbers of trials per session, including only sessions with non-zero spike counts in both L2/3 and L5/6. A total of 120 points are plotted with 20 values per session. Variation of ERN magnitude was predicted by variation of spike counts in L2/3 (highlighted by best-fit line) but not in L5/6.
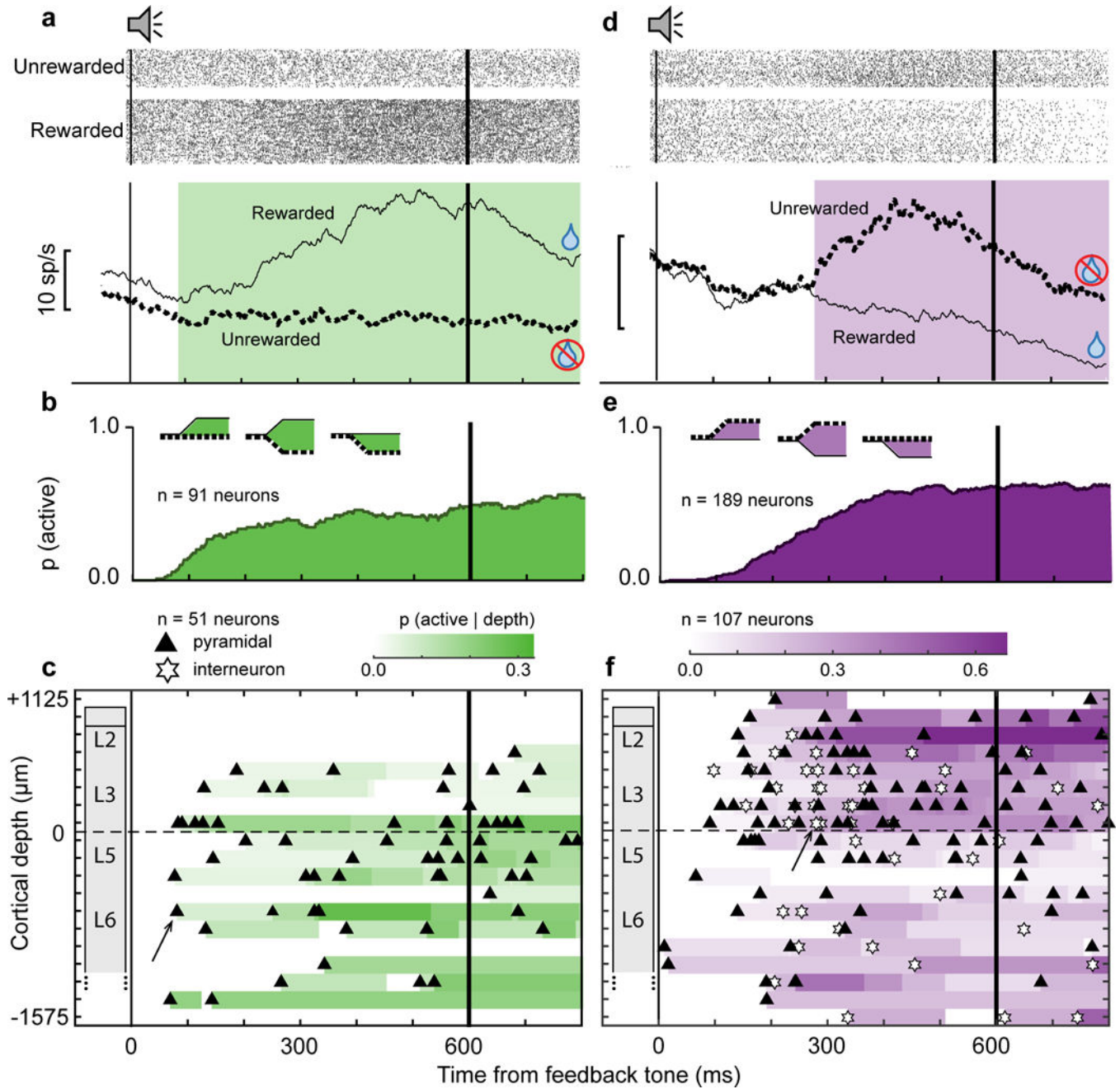
Fig. 4 |. Time-depth organization of reinforcement-related spiking in SEF.
a, Representative Gain neuron with greater discharge rate on rewarded (solid) relative to
unrewarded (dotted) trials following the feedback tone and around the time of fluid reward
delivery. This neuron was located in layer 6 and had a broad spike. Green highlights duration
of significant reward gain-related modulation. Rasters show activity for unrewarded and
rewarded trials. **b,** Recruitment of Gain neuron signal through time across all sessions,
which appeared either as facilitation on rewarded trials, suppression on unrewarded trials, or
both (inset). **c,** Time-depth plots showing latency and proportion of recruited Gain neurons
through time at each depth from perpendicular penetrations. Symbols mark beginning of

gain-related modulation for neurons with spike width 250 μm (black triangles) and <250 μm (white stars). The representative neuron in **a** is indicated by the black arrow. Color map indicates the percentage of neurons signaling gain through time at each depth. Dashed horizontal line marks L3-L5 boundary. The lower boundary of L6 is not discrete. **d,** Representative Loss neuron with greater discharge rate on unrewarded (dotted) relative to rewarded (solid) trials following the feedback tone and around the time of fluid reward delivery. This neuron was located in layer 3 and had a narrow spike. Purple highlights duration of significant reward loss-related modulation. Rasters show activity for unrewarded and rewarded trials. **e,** Recruitment of Loss neuron signal through time across all sessions, which appeared either as facilitation on unrewarded trials, suppression on rewarded trials, or both (inset). **f,** Time-depth plots showing latency and proportion of recruited Loss neurons through time and at each depth from perpendicular penetrations. Symbols mark beginning of loss-related modulation for neurons with spike width 250 μm (black triangles) and <250 μm (white stars). The representative neuron in **d** is indicated by the black arrow. Color map indicates the percentage of neurons signaling loss through time at each depth. Dashed horizontal line marks L3-L5 boundary. The lower boundary of L6 is not discrete.
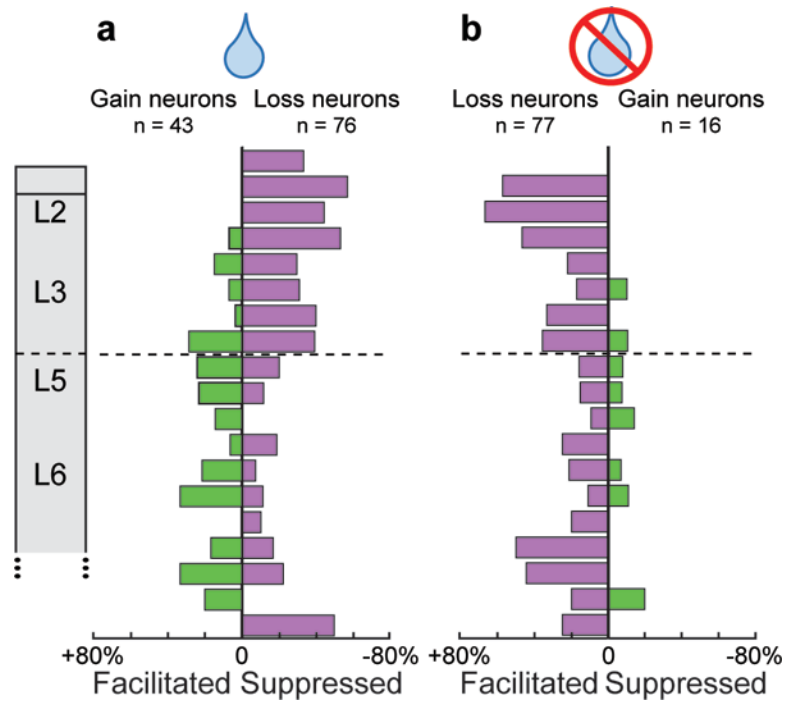
Fig. 5 |. Laminar structure of facilitation and suppression of Gain and Loss neurons.
a, Rewarded trials, laminar density of facilitated Gain (green) and suppressed Loss (purple) neurons. Facilitated Gain neurons were concentrated in L5/6. Suppressed Loss neurons were concentrated in L2/3. **b,** Unrewarded trials, laminar density of facilitated Loss neurons (purple) and suppressed Gain neurons (green) on unrewarded trials. Facilitated Loss neurons were concentrated in L2/3 and deep L6. Infrequent suppressed Gain neurons were concentrated in L5/6.
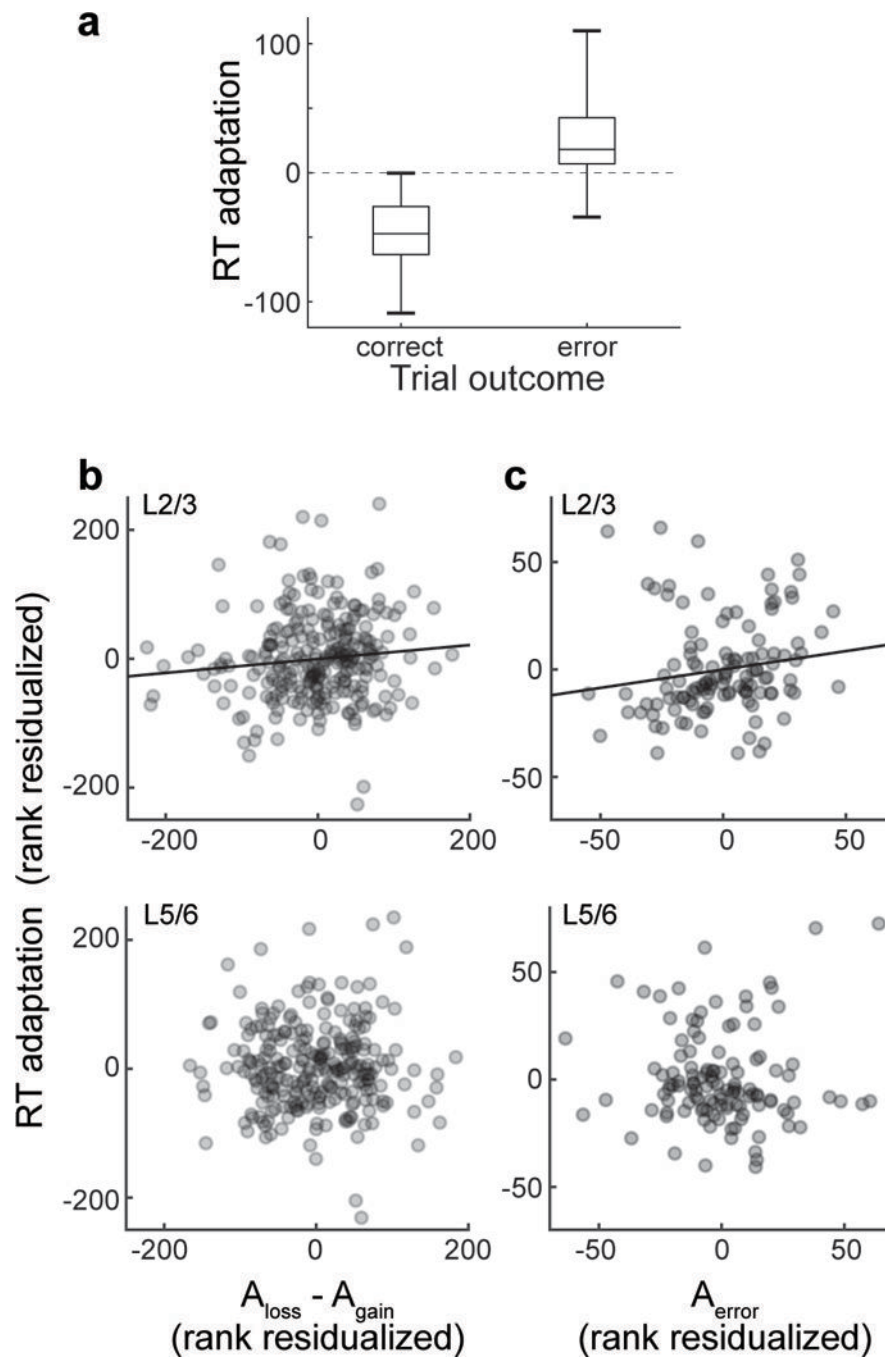
Fig. 6 |. Relationship between RT adaptation and layer-specific spiking activity.
a, Boxplot of RT adaptation, the difference in RT between successive trials, following correct and error trials across all 29 sessions, showing median (central line), first and third quartiles (box), and entire range of the data (whiskers). **b,** From 13 sessions with perpendicular penetrations, relationship between RT adaptation and spike count for Loss and Gain neurons ($A_{loss} - A_{gain}$) recorded in L2/3 (top) and L5/6 (bottom). Along the ordinate scale is plotted residual fixed-effects-adjusted rank of RT adaptation controlling for the ranks of fixed-effects-adjusted activity in the opposite layers and the probability of an error.

Along the abscissa is plotted the residual fixed-effects adjusted A_{loss} - A_{gain} rank in the identified layers controlling for the fixed-effects adjusted activity in the opposite layers and the probability of an error. Each point plots the average RT adaptation and associated spike count measure in one of 20 bins with equal numbers of trials per session; only sessions with non-zero spike counts in both L2/3 and L5/6 are included. A total of 260 points are plotted with 20 values per session. Variation in RT adaptation was predicted by variation of A_{loss} - A_{gain} in L2/3 (highlighted by best-fit line) but not in L5/6. **c,** From 6 sessions with perpendicular penetrations, relationship between RT adaptation and spike count for Error neurons (A_{error}) recorded in L2/3 and L5/6. Along the ordinate scale is plotted residual fixed-effects-adjusted rank of RT adaptation controlling for the ranks of fixed-effects-adjusted activity in the opposite layers and the probability of an error. Along the abscissa is plotted the residual fixed-effects adjusted A_{error} rank in the identified layers controlling for the fixed-effects adjusted activity in the opposite layers and the probability of an error. Each point plots the average RT adaptation and associated spike count measure in one of 20 bins with equal numbers of trials per session; only sessions with non-zero spike counts in both L2/3 and L5/6 are included. A total of 120 points are plotted with 20 values per session. Variation in RT adaptation was predicted by variation of A_{error} in L2/3 (highlighted by best-fit line) but not in L5/6.
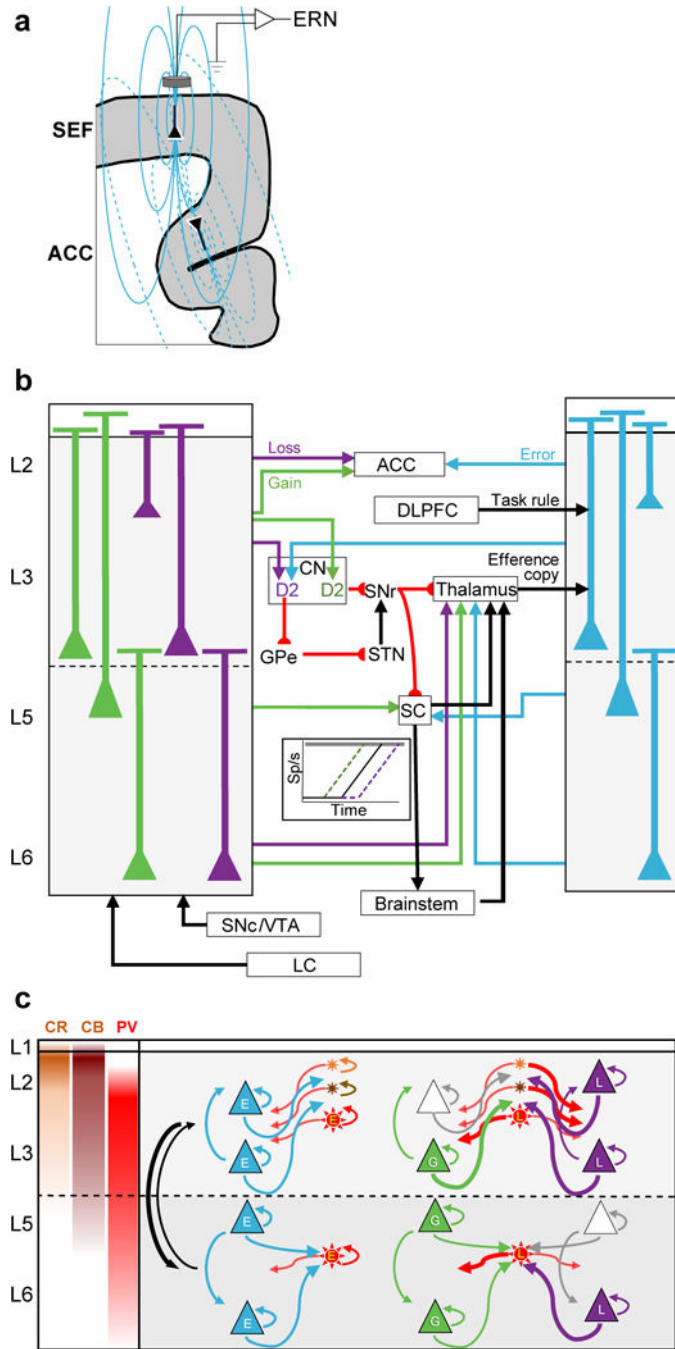
Fig. 7 |. Microcircuitry of SEF performance monitoring and executive control.
a, Coronal section of medial frontal cortex illustrating pyramidal neurons in SEF and dorsal ACC producing electric dipole moments and associated field lines contributing to the ERN from SEF (solid) and ACC (dotted). The dipole in dorsal ACC produces a field with polarity opposite that produced by SEF. How two such dipoles produce the ERN is unknown. **b,** Extrinsic circuitry for monitoring and executive control. The laminar distributions observed for Gain, Loss, and Error neurons are summarized with selected anatomical connections based on published studies. Gain and loss signals can arise in SEF through afferents from

substantia nigra pars compacta (SNc), ventral tegmental area (VTA), and locus coeruleus (LC)[37][38]. SEF can receive an efferent copy signal in afferents from the thalamus[39] and a task rule signal from dorsolateral prefrontal cortex (DLPFC) terminating in L2 and L3[40]. Conflict between the efferent copy and the task rule can cause error-related spiking in lower L3 and upper L5 neurons. Intracortical processing produces later activation of Error neurons in L2 and L6. L2/3 neurons project to nearby cortical areas like ACC[35] and thereby relay information about error and reward loss, which is registered later[8]. SEF projects to the caudate nucleus (CN)[35][36]. We conjecture that speeding or slowing of RT can be accomplished through the push-pull basal ganglia circuitry with direct pathway (D1) input from Gain neurons and indirect pathway (D2) input from Loss and Error neurons. The basal ganglia circuitry can advance or delay the onset of presaccadic accumulation in SC and FEF (inset diagram) that initiates a saccade when a threshold level is reached in the brainstem saccade generator, which innervates motor neurons[44]. Further details in text. **c,** Intrinsic microcircuitry for error and reinforcement processing. The laminar density of calretinin (CR, orange), calbindin (CB, brown), and parvalbumin (PV, red) neurons is indicated in left panel and summarized by the location of schematic neurons (stars). Schematic pyramidal neurons (triangles) are illustrated for L2, L3, L5, and L6. The most common depths observed or Error (E, cyan), Gain (G, green), and Loss (L, purple) are summarized by labeled pyramidal and putative PV neurons. Schematic arrows distinguished for each type of neuron indicate recurrent and interneuronal connections. Thick arrows indicate our conjecture about connections that explain the co-modulation of Gain and Loss neurons. Agranular cortex has weak interlaminar connectivity with stronger projections from L2/3 to L5/6. Further details in text.